The role of the stress-path and importance of stress history on the flow of water along fractures and faults; an experimental study conducted on kaolinite gouge and Callovo-Oxfordian mudstone

Robert J. Cuss, Jon F. Harrington, British Geological Survey, Keyworth, Nottingham, NG12 5GG, UK

Shanvas Sathar, Present address: Alberta Energy Regulator (AER), Centennial Place, 250 5th Street SW, Calgary - T2P 0R4, Alberta, Canada

Simon Norris, Radioactive Waste Management Limited, Building 587, Curie Avenue, Harwell Science and Innovation Campus, Didcot, Oxfordshire, OX11 0RH, UK

Jean Talandier, Andra, 1-7, rue Jean Monnet, 92298 Chatenay-Malabry, France

Corresponding author: R.J. Cuss, British Geological Survey, Keyworth, Nottingham, NG12 5GG, UK. (rjcu@bgs.ac.uk)

Key points:

- Importance of stress history on fracture flow.
- Stress dependency of fracture flow described by a power-law or cubic relationship.
- Fracture flow dependent on fracture roughness, thickness of gouge material, saturation state, permeability of the host material, clay mineralogy, and the degree of shearing.

Abstract: *The flow of water along discontinuities, such as fractures or faults, is of paramount importance in understanding the hydromechanical response of an underground geological disposal facility for radioactive waste. This paper reports four experiments conducted on kaolinite gouge on a 30° slip-plane and on realistic fractures created in Callovo-Oxfordian mudstone (COx) from France. Test histories were conducted that initially loaded the gouge material in step changes in vertical stress, followed by unloading of the sample in similar steps. This loading-unloading history showed considerable hysteresis in hydraulic flow, with only partial recovery of fracture transmissivity. This demonstrates the importance of stress history on fracture flow; consideration of just the current stress acting upon a fracture or fault may result in inaccuracies of predicted hydraulic flow. The stress dependency of fracture flow in both kaolinite and COx can be described by a power-law or cubic relationship, which is likely to be dependent on the fracture roughness, thickness of gouge material, saturation state, permeability of the host material, and clay mineralogy (i.e. swelling potential). The observed response of fracture transmissivity to normal stress in COx is a complex superposition of mechanical response of the fracture and the swelling of clay in the fracture surface. The stress-dependency of flow was also seen to be dependent on orientation with respect to bedding. A fracture perpendicular with bedding accommodates greater compression and results in a lower transmissivity. The orientation dependence is related to the anisotropic swelling characteristics of COx.*

Keywords

Fracture flow; multiphase flow; kaolinite; shear testing; stress history; Callovo-Oxfordian mudstone.

1. Introduction

Discontinuities (fracture, faults, joints, interfaces, etc.) play a key role in controlling the movement of water and gas around an underground Geological Disposal Facility (GDF) for radioactive waste. High Level Waste (HLW), Intermediate Level Waste (ILW) and some long-lived low-level radioactive waste and spent fuel are planned to be disposed of in a GDF within stable geological formations at depth (~200-800 m) by a number of countries. The disposal concept incorporates waste isolation and containment by engineered and geological barriers in such a facility. At depth the rock mass may be a naturally fractured environment, as in the case for crystalline rocks. The stress re-distribution resulting from the excavation of tunnels in both crystalline and clay-rich host rocks will result in the formation of the Engineered Disturbed Zone (EDZ), where an intricate range of discontinuity orientations are present in a complex localized stress field (Bossart *et al.*, 2002, 2004; Rutqvist *et al.*, 2009, Armand *et al.*, 2014). Therefore, most current disposal concepts will include a multitude of discontinuities as part of the natural and engineered environment, which will be present for varying time-scales dependent on the host-rock; i.e. the EDZ is likely to self-seal in a clay-rich formation, whereas it will persist for extended periods in a crystalline rock type. Depending on the *in situ* stress conditions and whether self-sealing has resulted in fracture closure, preferential pathways for fluid movement may form along any, all, or none of these discontinuities.

There are a number of potential events that may change the stress state that acts upon any fractures present in a GDF host rock. The modelling work of Barla and co-workers (Barla, 1999; Bonini *et al.*, 2001) showed that during the excavation of a tunnel the stress field is altered and the surrounding rock-mass follows a stress path. This results in changes in stress acting on existing discontinuities and, following their formation, a change in the stress acting on EDZ fractures. The process of closing a GDF is likely to be achieved by backfilling open spaces (access tunnels, etc.) with bentonite/sand mixtures or crushed host rock material (depending on disposal concept). This will result in swelling of clay-based materials on resaturation and the transmission of stress to the EDZ, resulting in a further change to the stress experienced by any discontinuities present in the host rock. Over geological timescales in certain parts of northern and northwestern Europe, there may be increased stress on the GDF as the result of glacial loading, or a reduction in stress as the result of erosion of some of the over-burden, although this is unlikely in France. Therefore, over the full history of the GDF several scenarios may occur that could result in changes in the stress acting upon discontinuities of varying time-scales.

The evolution of permeability in rocks under hydrostatic stress conditions has been widely reported. The stress dependency of permeability has been reported under hydrostatic stress conditions in a number of different rock types (e.g. Zoback & Byerlee 1975; Walsh & Brace 1984; Morrow *et al*., 1984; Neuzil *et al*., 1984; David *et al*., 1994; Dewhurst *et al*., 1999[1,2]; Katsube, 2000; Katsube *et al*., 1996[1,2]; Kwon *et al*., 2001; Zhang & Rothfuchs, 2004). However, in the field, rocks are subject to an inhomogeneous stress-field, where the vertical stress (determined by the weight of the overburden) exceeds the orthogonal maximum and minimum horizontal stresses (Holt, 1990). This has led to investigations of the sensitivity of matrix permeability to non-hydrostatic stress conditions, especially in sandstones (e.g.; Zhu & Wong, 1994; Zhu & Wong, 1997; Keaney *et al*., 1998). The reported permeability for intact shale, mudstones, and clay-rich rocks subjected to hydrostatic pressures varies from 10^{-16} m^2 to 10^{-23} m^2 (Kwon *et al*., 2001). Many researchers have shown that the permeability of shale decreases with externally applied stress (Neuzil *et al*., 1984; Katsube *et al*., 1996[1,2]; Dewhurst *et al*., 1999[1,2]; Katsube, 2000; Kwon *et al*., 2001;) and decreased porosity (Schloemer & Kloss, 1997; Dewhurst *et al*., 1998). A number of non-linear relationships have been proposed between permeability, porosity, and pressure in shale and mudstones, including exponential and power laws between permeability and pressure (Katsube *et al*., 1991; Dewhurst *et al*., 1999[1]).

The permeability, or transmissivity, of discontinuities and its associated relationship with stress has not been widely reported. The Compression of the Damaged Zone (CDZ) experiment conducted at the Meuse/Haute-Marne Underground Research Laboratory (URL) at Bure, approximately 300 km east of Paris, demonstrated that the transmissivity of fractures formed around the EDZ was sensitive to the loading experienced (de La Vaissière *et al.,* 2015). Only a small effect was seen in the transmissivity to gas, but clay/water interactions led to a decrease of water permeability of several orders of magnitude. In Opalinus Clay (OPA), the load plate experiment at the Mont Terri URL observed a fracture transmissivity decrease with increasing load pressures by up to a factor of 60 (Bühler *et al*., 2003). Careful experimental design proved that the decrease in transmissivity follows the stepwise increase of the load pressure and was due to mechanical compression of the fracture network. A longer-term reduction in transmissivity was also observed, which may be related to swelling and rearrangement of clay minerals. In the load plate experiment the transmissivity seen at the highest load was still greater than that for intact OPA. However, at the Meuse/Haute-Marne URL, permeability has been observed to return to that of the intact material within the uncertainty of water permeability for COx. Several laboratory experimental studies have been conducted examining fracture flow in Callovo-Oxfordian mudstone, including Davy *et al.* (2007), Foct *et al.* (2012), Zhang *et al.* (2013), and Auvray *et al.* (2015).

Gutierrez *et al*. (2000) experimentally investigated the hydromechanical behaviour of an extensional fracture in Kimmeridge Shale under normal and shear loading. At the time the fracture was created it had a higher permeability than the equivalent permeability of the intact shale. Increasing the contact normal stress across the fracture reduced the fracture permeability following an empirical exponential law. However, loading the sample to an effective normal stress twice as much as the intact rock unconfined compressive strength did not completely close the fracture, although it did reduce the permeability by an order of magnitude. Cuss *et al.* (2011) showed that fracture transmissivity in OPA decreased linearly with an increase in normal load over a limited stress range. This study also showed that shear movement along the fracture resulted in effective self-sealing in OPA and reduced hydraulic fracture transmissivity to similar levels to that of the intact material. A one order of magnitude reduction in fracture transmissivity of OPA just in response to re-hydration of the fracture because of the swelling of the clay minerals has been reported (Cuss *et al.*, 2014; Cuss & Harrington, 2014). A further order of magnitude reduction was observed in response to shearing along the fracture, this may be in part due to clay smearing and mineral rearrangement and/or due to a greater number of clay minerals coming into contact with water and swelling as a result of the formation of microfractures sub-parallel to the main fracture.

The objective of the current experimental program was to investigate the water flow properties of a discontinuity at 30° to changes in vertical load and to compare these observations with the recorded flow in a horizontal fracture formed in Callovo-Oxfordian mudstone (COx). This would simulate effective stress changes, such as pore-pressure variations on faults or stress changes associated with GDF closure. As stated above, the response of fracture flow to changes in normal stress are dependent on the rock-type that the fracture exists. Previous experimental work at the British Geological Survey (BGS) on fracture transmissivity in Opalinus Clay (Cuss *et al.*, 2011; 2014; Cuss & Harrington, 2014) showed that hydraulic flow is a complex, focused, transient property that is dependent upon normal stress, shear displacement, fracture topology, fluid composition, and clay swelling characteristics. The current experimental program aimed to extend this knowledge by investigating the influence of vertical stress on water flow through gouge-filled discontinuities and in COx. The response of discontinuities has two clear components; a mechanical response to load and a response from swelling effects of clay minerals. Comparing results from two experimental geometries would allow mechanical and swelling effects to be determined. The observations from the 30°discontinuity also are relevant to non-swelling fractures, such as those seen in crystalline environments.

2. Experimental setup

Experiments were performed using two similar bespoke shear apparatus, designed and built at BGS. The Direct Shear Rig (DSR, Figure 1a) was designed to study fracture transmissivity in clay-rich rock samples. The Angled Shear Rig (ASR, Figure 1b) was designed to study fault flow in a generic synthetic fault gouge at varying angles to the stress field.

Both the DSR and ASR are comprised of six key components:

1. Rigid steel frame that had been designed to deform as little as possible during the experiment;
2. Vertical load system comprising an Enerpac hydraulic ram that was controlled using a Teledyne/ISCO 260D syringe pump, a rigid loading frame and an upper thrust block (up to 20 MPa normal stress, 72 kN force). The Enerpac ram had a maximum stroke of 105 mm, which meant that it could easily accommodate the vertical displacement of the top block of the ASR as it rode up the fault surface at constant vertical load. Vertical travel of the thrust block was measured by a high precision non-contact capacitance displacement transducer, which had a full range of ± 0.5 mm and an accuracy of 0.06 μm;
3. Shear force actuator comprised of a modified and horizontally mounted Teledyne/ISCO 500D syringe pump designed to drive shear as slow as 14 microns a day at a constant rate (equivalent to 1 mm in 69 days) or as fast as 0.5 mm per second along a low friction bearing. The movement of the bottom-block was measured using a linear variable differential transformer (LVDT), which had a full range of ± 25 mm and an accuracy of 0.5 μm;

4. Pore pressure system comprising a Teledyne/ISCO 500D syringe pump that could deliver either water up to a pressure of 25.8 MPa. The syringe pump delivered water directly to the fracture surface;
5. A state-of-the-art custom designed data acquisition system using National Instruments LabVIEW™ software facilitating the remote monitoring and control of all experimental parameters;
6. A sample assembly, which was the main difference between the DSR and ASR. In both experimental setups, the bottom block was actively sheared and the top block was connected through a linkage system to a force gauge measuring the shear stress along the slip plane.
    a. DSR: two samples of 60 mm × 60 mm × ~25 mm were held by two stainless steel holders. Vertical load was applied to the rock samples by means of a steel thrust block. A 4 mm bore the same length as the upper fractured block delivered pore fluid through the top sample directly to the fracture surface.
    b. ASR: the sample assembly consisted of polished precision-machined 316 stainless steel top and bottom blocks (thrust blocks) with a dip of 30 degrees with respect to horizontal. Fluid was introduced through a 4 mm filter in the centre of the top block. Two additional 4 mm diameter filters positioned orthogonally to each other at 15 mm from the central pore fluid inlet were connected to pore-pressure transducers in order to monitor pressure within the gouge (see Figure 1b). The lower thrust block was longer than the 60 mm × 60 mm upper thrust block in order to maintain a constant contact area during shearing. Two high precision eddy current non-contact displacement transducers were located either end of the top thrust block and recorded gouge thickness directly and determined

non-parallel alignment of the two thrust blocks. These submersible devices had a full range of ± 1 mm and an accuracy of 0.2 µm.

2.1 Test material and experimental protocols

For the tests conducted using the DSR, a sample of Callovo-Oxfordian mudstone[1] (COx) was used from material extracted from the Meuse/Haute-Marne underground research laboratory at Bure in France. Yven *et al.* (2007) report three main mineral phases; clay minerals, quartz and calcite. Secondary mineral phases include dolomite, feldspar, pyrite, hematite and traces of siderite. Calcite and quartz represent 40 – 55% of the rock. Clay represents 20 – 55%, with secondary minerals forming less than 5%. Clay minerals include illite and illite-smectite with subordinate kaolinite and chlorite. Upon receipt of the preserved core barrels at BGS, the material was catalogued and stored under refrigerated conditions of 4°C to minimize biological and chemical degradation. The preserved core barrels consisted of a multi-layered arrangement designed to re-stress the core to *in situ* stress and to environmentally seal it in order to reduce chemical, biological and drying effects. Both test samples were prepared from core material from borehole OHZ1607, which was drilled horizontal to bedding with a diameter of 100 mm. Table 1 summarizes the origin of the core material and the properties of the test samples. The test samples were prepared by dry cutting an approximate 60 × 60 × 50 mm block from core barrel material. The faces were ground flat and parallel using a diamond mill so as produce a good fit into the sample holders. The starting water saturation is reported in Table 2, along with the geotechnical properties of the starting material. The samples were wrapped in cling-film and between test stages were stored in two sealed bags to reduce the possibility of drying.

---

[1] The Callovo-Oxfordian mudstone (COx) from the Meuse/Haute-Marne URL is often referred to as the Callovo-Oxfordian claystone. However, it does not always consist of clay minerals greater than 50 % volume and as such is not necessarily a true claystone. Therefore, the term mudstone is used. Please note COx is also referred to as Callovo-Oxfordian claystone/argillite/formation/clay rock/mudstone/argillaceous rock/shale.

A fracture was created in the cubic sample by shearing in the DSR apparatus. As the sample was rigidly held by two steel holders, the shearing action resulted in a realistic fracture being formed at the junction between the two holders. This created two samples of approximately 25 mm thickness. A bore of 4 mm diameter was drilled in the top fracture sample in order to accommodate the pore injection pipe of the upper thrust block. During fluid injection a chemically balanced synthetic pore fluid was used similar to that found at Bure (Gaucher *et al.*, 2007). This was manufactured at BGS with the following composition: 227 mg l^{-1} Ca^{2+}, 125 mg l^{-1} Mg^{2+}, 1012 mg l^{-1} Na^{+}, 35.7 mg l^{-1} K^{+}, 1240 mg l^{-1} Cl^{-}, 1266 mg l^{-1} SO_4^{2-}, 4.59 mg l^{-1} Si, 9.83 mg l^{-1} SiO_2, 13.5 mg l^{-1} Sr, 423 mg l^{-1} total S, and 0.941 mg l^{-1} total Fe.

Following fracture creation, the two fracture surfaces were scanned using a NextEngine 3D Scanner HD. This produces a 3D mesh model of the fracture surface accurate within an error of ± 65 microns. Algorithms inbuilt within the data acquisition ScanStudio HD software produced clean surface data which were used in subsequent empirical and statistical analysis. Fracture roughness and other standard measurements were made using TrueMap 5.0 surface topography software. A small quantity of disaggregated clay may have been lost during the scanning process, although this was minimal, with only a few milligrams of clay dislodged from the fracture surface. The fracture surfaces were exposed to air for a maximum of five minutes during scanning and were placed in sealed sample bags at all other times. This was to reduce moisture loss, which over this short period of time is assumed to be negligible.

For tests conducted using the ASR, a gouge material for the experiments was prepared from powdered kaolinite (Supreme Powder); 16 ± 0.1 g of de-ionized water was added to 20 ± 0.1 g of kaolinite powder. The water and kaolinite were then stirred for five minutes giving a kaolinite paste with a gravimetric water content of 80 ± 1%, or a saturation state close to 100% (see Table 2). The paste was smeared uniformly onto the surface of the top block, which was then carefully lowered onto the bottom block thus forming a kaolinite paste gouge. The initial thickness of the gouge was determined to be of the order of one millimetre. However, as no lateral confinement was made of the clay gouge, thickness decreased to approximately 70 ± 10 μm with loading and clay was squeezed from between the thrust blocks. The apparatus was designed without lateral gouge confinement as this would require sealing elements that would have a high frictional component along the fault surface compared with the low frictional properties of kaolinite. Initial loading resulted in excess clay being squeezed out from the fault surface; this excess material prevented water from the shear bath entering the fault gouge or from causing sloughing.

In the ASR, a constant pore pressure of approximately 1 MPa was created carefully once a small vertical stress had been imposed on the fracture surface. Care was taken to ensure that kaolinite was not eroded from the slip plane by limiting flowrate to sub-100 μl h^{-1}. At low normal stresses, the fractures in COx could not be limited to 100 μl h^{-1} at such a high pore-pressure. For test DSR_COx_01, pore pressure was slowly increased in steps from 120 kPa to 500 kPa during the hydration stage, with 750 kPa used during the flow test. At all steps flow was kept below sub-500 μl h^{-1}. For test DSR_COx_02 an initial flow rate of 100 μl h^{-1} was imposed until a pore pressure of 150 kPa was achieved, all further testing was then undertaken at a constant pore pressure of 150 kPa. All measures were taken to limit erosion of clay from the fracture surfaces in all tests. Once stable flow had been achieved, the vertical stress was increased (or decreased) in regular steps. The flow rate of the injection system was monitored and used to determine fracture transmissivity.

2.2 Data reduction

Fracture transmissivity was calculated assuming radial flow from the injection hole given the steady state fluid flow rate Q and the pressure head H at the injection point. Steady flow in a cylindrical geometry is given by:

$$Q = \frac{2\pi T(h_i - h_0)}{\ln(r_o) - \ln(r_i)} \qquad [1]$$

where T is the transmissivity, h_i is the head on the inner surface with radius r_i, and h_o is the head on the outer surface at radius r_o (Gutierrez *et al.*, 2000). For the experimental setup r_0 = 30 mm, r_i = 1.96 mm, h_0 = 0.05 m and h_i ~ 100 m. Substituting these constants into equation 1 gives transmissivity (m^2 s^{-1}):

$$T = 1.183 \times 10^{-12} \frac{Q}{P_p} \qquad [2]$$

if the fluid flux (Q in µl h^{-1}) and pore pressure (P_p in kPa) are known. This relationship was used to calculate the transmissivity of the fracture throughout the experiment. It should be noted that Equation 1 relates to a circular sample, whereas the fracture is created in a cubic sample. Therefore, it is assumed that the shortest distance between the injection point and the edge of the sample is the controlling factor. It should also be noted that as the fracture is sheared the contact area between the top and bottom face of the fracture reduces. As a result, the shortest distance to the edge of the sample (r_o) effectively reduces. Scoping calculations showed this had a negligible effect on the overall calculation.

3.0 Experimental results for Angled Shear Rig (Kaolinite gouge)

Two load-unload experiments were conducted using the ASR apparatus with water as the injection fluid, both on a 30° slip-plane (Table 2). Figure 2 shows an example of the data recorded during hydraulic flow for test ASR_Tau05_30wLU plotted against time, whereas data plotted against vertical stress are shown in Figure 3. Vertical stress was sequentially increased in stages of 0.2 MPa per day from an initial 0.2 MPa to a maximum vertical stress of 2.6 MPa (Figure 2b). The pore fluid injection pressure was maintained at a constant value of 1 MPa. Although no horizontal stress was applied, the increase in horizontal stress as a consequence of vertical stress increase was logged throughout the duration of the experiment. During the unloading stage, the vertical stress was decreased in steps of 0.2 MPa from 2.6 MPa to 0.2 MPa. Temperature remained uniform at 20.5 ± 0.1°C throughout the entire duration of the experiment (Figure 2a). The flow rate decreased an order of magnitude from 50 µl h^{-1} to 5 µl h^{-1} during loading from 0 to 2.6 MPa. During unloading from 2.6 to 0.2 MPa, flow rate doubled from 5 µl h^{-1} to 10 µl h^{-1}. From 2.6 MPa to 1.0 MPa vertical stress, the flow rate remained constant at 5 µl.h^{-1} irrespective of the significant reduction in vertical load (Figure 2c, Figure 3a). Pore pressure within the slip plane recorded much lower pressures (50 – 80 kPa and 5 – 25 kPa) than the injection pressure (1 MPa) (Figure 2d). During loading, fracture transmissivity decreased from 5×10^{-14} m^2 s^{-1} to 0.6×10^{-14} m^2 s^{-1}. However, during unloading transmissivity recovered to only 1.1×10^{-14} m^2 s^{-1}. The thickness of the kaolinite gouge decreased with loading from 54 µm at a vertical stress of 0.2 MPa to 42 µm at a vertical stress of 2.6 MPa. During unloading, the slip plane width continued to decrease further to 40 µm before finally recovering to 43 µm after full unloading (Figure 2e, Figure 3b). Vertical displacement was seen to reduce by nearly 350 µm during the loading stage, with a hysteretic recovery during unload (Figure 2f, Figure 3c). No significant differences were seen between tests ASR_Tau05_30wLU and test ASR_Tau01_30wLU, as shown in Cuss *et al.* (2013).

Figure 4 shows the results of flow achieved for the two tests conducted injecting water into a 30° discontinuity during loading from 0.1 to 2.6 MPa and unloading from 2.6 to 0.2 MPa. As can be seen, the starting flow rates of the two tests were different by nearly a factor of 2. Both tests were setup in identical ways using the same pre-mixed weight of kaolinite and deionised water. The difference is likely to be related to differences in gouge thickness. As normal load was increased in steps, the flow along the slip plane steadily reduced. In both experiments, although starting from dissimilar flow rates, a flow rate of approximately 6 µl h^{-1} at a vertical stress of 2.6 MPa was achieved. As both experiments resulted in a similar flow, it is suggested that the final gouge thickness was similar for both tests following expulsion of excess clay during loading. The difference may also be due to variation in starting saturation of the kaolinite gouge, although every care was taken to produce gouge material that was identical. As reported in Cuss *et al.* (2013), shear is seen to be an effective self-sealing mechanism in kaolinite gouge, significantly reducing flow. Therefore, differences in starting transmissivity may also be related to the degree of shearing experienced during the setting up of the experiment. On unloading, this flow rate did not significantly alter until a vertical load of approximately 0.75 MPa was reached.

3.1 Experimental results for Direct Shear Rig (COx)

Two experiments were conducted using the DSR on samples of COx, as described in Table 2. The first test (DSR_COx_01) was a simple loading history in order to describe the stress dependency of fracture transmissivity. The second test (DSR_COx_02) was a more detailed load-unload-reload test history. It should be noted that the orientation of the two tests were different, with test DSR_COx_01 fractured parallel to bedding, while DSR_COx_02 was fractured perpendicular to bedding.

The results from the first test that was performed are shown in Figure 5. The test history is shown as two separate tests due to the behaviour recorded. Previous testing conducted in Opalinus Clay (e.g. Cuss *et al.*, 2011) showed that the injection of pore fluid or the change in normal load resulted in a transient response in fracture transmissivity that would equilibrate within a few days. As shown in Figure 5e, the initial test step showed a short transient, giving an average flow rate of 99 μl h^{-1} at 2.07 MPa after 72 hours. Normal load was increased to 2.5 MPa and a considerable transient was observed. As clearly seen, a full asymptote of the flow rate had not been achieved after 1,512 hours (2 months). As well as a continually changing response for flow, a small component of normal displacement was seen that similarly had not reached equilibrium (Figure 5g). It was not feasible to continue the experiment at such a slow rate and the decision was taken to begin a new phase of experimentation with step changes in normal load being conducted on 24-hour periods. This was deemed sufficient to allow the transient associated with a change in normal load to equilibrate and to be a good representation of the mechanical change in flow properties without the influence of long-term changes in flow properties associated with clay swelling. This phase of experimentation is shown in Figure 5b,d,f,h. Results shown in Figure 5b are affected by the air conditioning in the laboratory, which was not stable at the time these results were collected due to an intermittent fault (this fault affected no other experiments). Overall, air conditioning issues did not have a detrimental influence on flow in relation to results shown in Figure 5f, although a short-term variation is seen. It was still possible to determine an average flow for each normal load step. During the full duration of the experiment, flow reduced from 100 µl h^{-1} at 2.07 MPa to 40 µl h^{-1} at 3.85 MPa. Figure 8 shows that a good relationship was observed with a decreasing fracture transmissivity from 1.6×10^{-13} m^2 s^{-1} to 4.2×10^{-14} m^2 s^{-1} as normal load increased from 2 to 3.85 MPa.

Figure 6 shows the data recorded during hydraulic flow test DSR_COx_02 during a load-unload-reload (LUR) history plotted against time, data plotted against normal stress is shown in Figure 7. Normal stress was sequentially increased in steps of 0.15 or 0.4 MPa from an initial 0.54 MPa to a maximum normal stress of 1.67 MPa (Figure 6b). Each step was conducted until flow rate stabilized and ranged in duration from 1 to 24 hours. Due to high flow rates seen at low normal stresses, the pore fluid injection pressure was maintained at constant values of between 0.15 and 0.25 MPa, as shown in Figure 6b. During the unloading stage, the normal stress was decreased in steps of 0.25 or 0.45 MPa from 1.67 MPa to 0.53 MPa. The reload stage saw normal stress increased in steps of between 0.2 and 0.45 MPa from 0.53 MPa to a new maximum normal stress of 3.42 MPa. Temperature remained uniform at 21.25 ± 0.1 °C throughout the entire duration of the experiment (Figure 6a).

The early flow rate history was very complex (Figure 6c, Figure 7a). The observations stated above for tests conducted on kaolinite gouge showed a distinct hysteresis during unloading; therefore, it was vital that normal load was increased from a starting low normal stress. This was complicated by issues related to erosion along the fracture surface and the necessity to ensure that excessive flow rates were not sustained. This resulted in variations in pore injection pressure and duration of stages. Post experiment examination of the sample did not highlight any features of erosion on the fracture surface. The initial stage had a high flow rate of 1,600 µl h^{-1} at 0.54 MPa, which reduced to 142 µl h^{-1} at 1.67 MPa. During the unloading stage there was a partial recovery of flow to 257 µl h^{-1} as normal stress was reduced to 0.53 MPa. During reloading to the previous maximum normal stress of 1.67 MPa the flow reduced to 120 µl h^{-1}, which is similar to the flow rate that was recorded at the end of the initial loading phase. As normal stress was increased to the new maximum of 3.42 MPa the flow rate reduced to 7.3 µl h^{-1}. Therefore, during the duration of the experiment the fracture transmissivity reduced from 1.3×10^{-11} m^2 s^{-1} to 5.7×10^{-14} m^2 s^{-1}. Figure 6d and Figure 7b show the results for normal displacement. As shown, a near linear reduction in normal displacement was observed during loading, with a small degree of hysteresis seen on unloading. Only 0.25 mm of normal displacement was seen during the full test history.

4 Discussion

The current study has utilized both kaolinite gouge as an analogue fracture and a shear fracture created in COx. The use of a kaolinite gouge was in order to reduce the number of variables in the experiments by effectively eliminating fracture roughness and the presence of asperities. The selection of kaolinite was determined by the low swelling capacity of the clay, facilitating quicker experiments and the study of a greater number of features of fracture flow. The limited swelling capacity also means that the fluid flow behaviour is dominated by the mechanical response of flow to loading. In contrast, COx has a high content of swelling clay (illite and illite-smectite), which means that observations listed above are a combination of the mechanical response of loading and the swelling response of the clay minerals on the fracture surface. However, comparisons can still be made in the behaviour observed in both kaolinite and COx fractures, with the kaolinite results aiding the separation of mechanical and swelling responses in COx. Figure 8 shows that when viewed in log vertical stress versus log fracture transmissivity space, linear regions of the data are clearly defined, signifying a power-law relationship between stress and fracture transmissivity for all the current tests.

As seen in Figure 8, the only exception to the power-law behaviour is test DSR_COx_02, although this discrepancy can be explained. As stated earlier, the initial test history was dominated by the need to minimize flow through the fracture and to ensure that erosion of the fracture surface did not occur. The created fracture would have had mismatch between the fracture surfaces, resulting in asperities and a higher transmissivity than for a perfectly matched fracture surface. As vertical stress was increased in the experiment, these asperities became less dominant and flow reduced, and during this phase of the test history a linear relationship can be used to describe the dependence of transmissivity on stress. During this period of the test, swelling would also have been a dominant process and the necessity to keep test stages short meant that full equilibration per stage had not been reached. However, at approximately 1.7 MPa vertical stress, the behaviour changed: at this stress level the asperities have closed and the fracture began to show a power-law relationship between stress and flow. This transition was not seen in test DSR_COx_01 for two reasons. Firstly, the minimum stress exceeded 2 MPa, therefore asperities created by mismatch may have closed. Secondly, the first stage of the test resulted in a prolonged period of rehydration and swelling on the fracture surface may have caused the mismatch to have been sealed.

Close examination of test data for DSR_COx_02 suggests that a further change in behaviour may have happened at around 2.75 MPa. This can be interpreted as a slip event on the fracture surface. The increasing vertical stress has become sufficient that the mismatch has resulted in a small movement along the fracture. Shear has been shown to be an effective self-sealing mechanism in fracture experiments (e.g. Cuss *et al.*, 2011; 2013; 2014) and this would result in a decrease in fracture transmissivity. Close examination of all recorded data is not conclusive on whether movement occurred or not. However, a decline in shear stress around this time suggests movement did occur. Therefore, the alternative power-law fit shown in Figure 8a and Table 3 is more representative of the relationship between stress and flow. It has to be acknowledged that true steady-state conditions were not achieved in all test stages and that as well as the mechanical closure of the fracture there is an ongoing reduction in flow related to self-sealing and swelling of clay minerals. These observations are in contradiction to the CDZ field test (de La Vaissière *et al.*, 2015).

Berkowitz (2002) extensively reviewed flow though fractures and fractured rocks. Several models of relationships of fracture flow with increasing normal stress exist, based on linear, cubic, exponential and power-laws. During the current study, no appraisal has been made of the validity of the available models. However, as shown in Figure 9 and Table 4, the data from the current study have been fitted using a range of empirical relationships between flow and vertical stress. In Table 4 the highlighted values represent the relationships that have the highest value of R^2 and therefore are statistically the best fit to the data, although this approach does not necessarily represent the best fit to the data in a physical sense. All relationships (power-law, exponential, logarithmic and cubic) offer a good approximation of the data, although the linear relationship is poor in most tests. It can be seen that a cubic relationship offers the best fits to the loading data, although good fits are achieved with power-law, exponential and logarithmic relationships. Both cubic and power-law relationships offer good descriptions of the flow behaviour during unloading. Table 4 suggests that a cubic relationship best describes the flow properties of fractures during loading and unloading.

Figure 9c shows data from the CDZ (Compression of the Damaged Zone) in situ experiment conducted at the Meuse/Haute-Marne URL (de La Vaissière *et al.*, 2015). Data is shown for boreholes CDZ1305 and CDZ1306, which were behind a hydraulic loading plate installed in the GET drift. The hydraulic ram loaded the walls of the tunnel and resulted in the closure of the damage zone around the tunnel. As shown, data for conductivity at different loading stresses are also well described by a cubic law. These data are not well described by a power-law relationship. Therefore, a cubic law describes the relationship between loading and flow seen in Callovo-Oxfordian mudstone.

The current study has highlighted the significance of stress history with the non- or partial-recovery of flow during unloading. In all tests that included unloading stages, irrespective of whether gouge or fractured rock was used, a memory of the maximum load experienced was retained. This is evidenced by considerable hysteresis on the unloading cycle of the test history (Figure 4, Figure 7, Figure 8b). The unloading response can also be seen to be described by a power-law or cubic relationship. For COx, a power-law of 18.5 $\sigma_n^{-0.6}$ is observed. The situation for kaolinite gouge is somewhat different. Initially there is no recovery of flow, until at a threshold vertical stress the flow recovers as described by a power-law. However, a cubic relationship adequately describes the full unload response. Similar hysteresis has been noted in Opalinus clay (Cuss *et al.,* 2011; 2014). The unload history of three tests are shown in Figure 10. The data for Opalinus clay (Cuss *et al.*, 2011) were not originally reported in terms of hysteresis. However, a reinterpretation of the data shows the initial testing state was to increase vertical stress to a maximum value and measure flow during unloading steps. As shown, little recovery of flow was experienced. Figure 10 also shows hydraulic flow data measured on fractured COx within an isotropically loaded test configuration (COx_4; Harrington *et al.*, 2017). This dataset was also measured from a maximum stress state in lowered stress steps and can be defined by a power-law relationship. The observation of such behaviour in tests conducted in isotropic and shear test configurations demonstrates that the power-law unloading response is not purely an artefact of the test geometry used.

The observation of hystersis can be explained using classical soil mechanics. The loading stage of the fracture follows the virgin consolidation line (VCL) with the change in flow described by a power-law relationship. Unloading follows the rebound reconsolidation line (RRL), with a partial recovery of flow properties, due mainly to a recovery in void ratio in response to a lowering of stress. However, in all tests described there are considerable differences seen at stress levels depending on whether observed during a loading or unloading stress state. This illustrates the importance of stress history on predicting flow along discontinuities and has been used to explain the non-applicability of the critical stress approach in its simple form for a UK site (Sathar *et al.*, 2012). Other processes, such as surface charge of clay minerals opposing recovery of porosity on unloading and non-recovery of flow related to clay swelling in response to increasing stress changes, may also be contributing to the observed hysteresis; these processes require further investigation. Therefore, stress history is an important control on fracture flow and consideration only of the current stress state may lead to inaccuracies in the prediction of flow in fractured mudrocks.

Figure 8 shows that a power-law can describe the relationship between flow and vertical stress for COx. Different slopes are noted, as are different intercepts. For instance, at 3 MPa vertical stress the fracture transmissivity is 6.8×10^{-14} m^2 s^{-1} for test DSR_COx_01 compared to 1.9×10^{-14} m^2 s^{-1} for test DSR_COx_2. This difference can be attributed to the orientation of the test samples, or may be due to the difference in durations of test stages in the two experiments. Test DSR_COx_01 was orientated with a fracture parallel to the bedding, whilst test DSR_COx_02 was fractured perpendicular to bedding. These differences are also noted in the vertical displacement (dilation/contraction of the fracture) seen during the experiment. For test DSR_COx_01, a total of 0.07 mm of displacement was noted, whereas nearly 0.25 mm was seen in test DSR_COx_02. This suggests that a fracture perpendicular with bedding accommodates greater compression and explains why a lower fracture transmissivity is observed. The swelling characteristics are also dissimilar between the tests. As stated earlier, test DSR_COx_01 showed a considerable time-dependent response early in the test history, suggesting that a fracture parallel to bedding exhibits greater time-dependent swelling compared with a fracture oriented perpendicularly. Test DSR_COx_02 would be expected to show greater swelling characteristics given a lower starting saturation of the test sample. These results show that fracture orientation with respect to bedding may play a role on the flow properties, both magnitude and stress sensitivity of flow. However, it has to be acknowledged that the test histories of the two experiments are considerably different and the super-position of mechanical and swelling responses may be the cause of these observations.

Comparisons can be made between the current experiments and those conducted on fractures in Opalinus Clay (OPA). Cuss *et al.* (2009; 2011) describe the variation of fracture flow dependence on normal stress for an idealized planed fracture in OPA. A hydraulic transmissivity of approximately 5×10^{-14} m^2 s^{-1} was observed, which is comparable with the $0.5 – 6 \times 10^{-14}$ m^2 s^{-1} seen in the current study for kaolinite and $0.8 – 16 \times 10^{-14}$ m^2 s^{-1} seen in COx.

The current study has shown that hydraulic flow along fractures within the engineering disturbed zone (EDZ) surrounding an underground geological disposal facility for radioactive waste in Callovo-Oxfordian mudstone will have a stress-dependent response. This can be defined by a cubic-law relationship for either individual fractures, as determined from laboratory experiments, or for the bulk rock mass, as determined from *in situ* experiments. Fracture flow reduces as the stress acting across a fracture increases. Therefore, swelling of Callovo-Oxfordian mudstone or engineered sealing components will result in a reduction in flow and if sufficient, this will reduce to that seen in the intact rock. This study also showed that the flow along EDZ fractures will have a stress-memory and will be similar to the maximum stress that has been experienced by the rock. This hysteresis means that future reductions in loading of the rock will not resort in significant recovery of enhanced flow.

5. Conclusions

This paper describes an experimental study of four loading-unloading experiments conducted on kaolinite gouge on a 30° slip-plane and shear fractures created in COx. The main conclusions of the study are:

a. The observed response of fracture transmissivity to normal stress in COx is a complex superposition of mechanical response of the fracture and the swelling of clay in the fracture surface;
b. During a loading (vertical stress) and unloading cycle, hysteresis in flow was observed signifying the importance of stress history on fracture flow. Consideration of just the current stress acting upon a fracture, and not a history of stress variation, may therefore result in an inaccurate prediction of hydraulic flow;
c. The stress dependency of fracture flow in both kaolinite and COx can be described by a power-law or cubic relationship. Sufficient data are not yet available to fully understand the physical controls on the parameters of the relationship observed;

d. During unloading stages only partial recovery of flow was observed in kaolinite and COx. This partial recovery of flow has been observed in isotropically-loaded samples and shows that the behaviour is not a simple artefact of the test geometry;

e. COx showed a considerable time-dependent behaviour, indicating that it has a good self-sealing potential as clay minerals swell once they are hydrated;

f. Fracture orientation with respect to bedding may play a role on flow properties, both magnitude and stress sensitivity of flow. A fracture parallel with bedding accommodates greater compression and results in a lower transmissivity;

g. Observations of flow within a clay-filled gouge showed a consistent behaviour to the mechanical response seen for COx, showing that the simplified experimental geometry effectively replicated the flow observed in real fractures. However, the addition of swelling in COx gives a more complex stress-dependent flow.

Acknowledgements

The study was undertaken by staff of the Minerals and Waste Program of the BGS using the experimental facilities of the Transport Properties Research Laboratory (TPRL). Funding for the study was provided by Agence Nationale pour la Gestion des Déchets Radioactifs (Andra), the Nuclear Decommissioning Authority – Radioactive Waste Management Directorate (NDA-RWMD; now the Radioactive Waste Management Limited, RWM), the European Union (FORGE Project; Grant Agreement nº230357) and the British Geological Survey. The authors would like to thank the skilled staff of the Research & Development Workshops at the BGS, in particular Humphrey Wallis, for their design and construction of the experimental apparatus. This paper is published with the permission of the Director, British Geological Survey (NERC). The data from this paper are available from BGS.

References

Armand, G., Leveau, F., Nussbaum, C., de La Vaissiere, R., Noiret, A., Jaeggi, D., Landrein, P., and Righini, C. (2014) Geometry and properties of the excavation-induced fractures at the Meuse/Haute-Marne URL drifts. *Rock Mech Rock Eng* 2014; **47**(1): pp.21–41.

Auvray, C., Morlot, C., Fourreau, E. and Talandier, J. (2015) X-Ray Tomography Applied to Self-Healing Experiments on Argillites. In *13th ISRM International Congress of Rock Mechanics*. International Society for Rock Mechanics.

Barla, M. (1999) Tunnels in swelling ground: Simulation of 3-D triaxial tests by triaxial laboratory testing. PhD Thesis, Technical University of Turin, Italy, 179p.

Berkowitz, B. (2002) Characterizing flow and transport in fractured geological media: A review. *Advances in water resources*, **25**(8), pp.861-884.

Bonini, M. Barla, M. and Barla, G. (2001) Flac applications to the analysis of swelling behaviour in tunnels. 2nd Flac Symposium on Numerical Modeling in Geomechanics, Lione, 29-31 October, 2001

Bossart, P., Meier, P. M., Moeri, A., Trick, T., and Mayor, J.-C. (2002) Geological and hydraulic characterisation of the excavation disturbed zone in the Opalinus Clay of the Mont Terri Rock Laboratory. Engineering Geology, 66 (1-2), pp. 19-38.

Bossart, P., Trick, T., Meier, P.M. and Mayor, J.C. (2004) Structural and hydrogeological characterisation of the excavation-disturbed zone in the Opalinus Clay (Mont Terri Project, Switzerland). *Applied clay science*, *26*(1), pp.429-448.

Bühler, C., Heitz, D., Trick, T., and Frieg, B. (2003) In-Situ Self-Sealing of the EDZ as a Consequence of Loading. In: Davies, C and Bernier, F. (Eds.) Impact of the Excavation Disturbed or Damaged Zone (EDZ) on the Performance of Radioactive Waste Geological Repositories. Proceedings of a European Commission CLUSTER Conference and Workshop Luxembourg, 3 to 5 November 2003. EUR 21028 EN pp.281-286.

Cuss, R.J. and Harrington, J.F. (2014) Experimental observations of the flow of water and gas along fractures in Opalinus Clay. Extended abstract We07. Fourth EAGE Shale Workshop, 6-9 April 2014, Porto, Portugal.

Cuss, R.J., Graham, C.C., Wiseall, A.C, and Harrington, J.F. (2016) Cyclic loading of an idealized clay-filled fault; comparing hydraulic flow in two clay gouges. *Geofluids*, **16**, pp.552-564. DOI: 10.1111/gfl.12175.

Cuss, R.J., Harrington, J.F., Milodowski, A.E., and Wiseall, A.C. (2014). Experimental study of gas flow along an induced fracture in Opalinus Clay. British Geological Survey Commissioned Report, CR/14/051. 79pp.

Cuss, R.J., Milodowski, A., and Harrington, J.F. (2011) Fracture transmissivity as a function of normal and shear stress: first results in Opalinus clay. Physics and Chemistry of the Earth. 36, pp. 1960-1971.

Cuss, R.J., Milodowski, A.E., Harrington, J.F. and Noy, D.J. (2009) Fracture transmissivity test of an idealised fracture in Opalinus Clay. British Geological Survey Commissioned Report, CR/09/163. 74pp.

Cuss, R.J., Sathar, S., and Harrington, J.F. (2012) Fracture transmissivity test in Opalinus Clay; test conducted on a realistic fracture. British Geological Survey Commissioned Report, CR/12/132. 52pp.

Cuss, R.J., Sathar, S., and Harrington, J.F. (2013) Final Report of FORGE WP4.1.2: Validation of critical stress theory applied to repository concepts. British Geological Survey Commissioned Report, CR/13/001. 96pp.

David, C., Wong, T.F., Zhu, W., and Zhang, J. (1994) Laboratory measurement of compaction-induced permeability change in porous rocks; implications for the generation and maintenance of pore pressure excess in the crust. Pure and Applied Geophysics, 143, pp. 425-456.

Davy, C.A., Skoczylas, F., Barnichon, J.D. and Lebon, P. (2007) Permeability of macro-cracked argillite under confinement: gas and water testing. *Physics and Chemistry of the Earth*, Parts A/B/C, **32**(8), pp.667-680.

de La Vaissière, R., Armand, G., and Talandier, J. (2015) Gas and water flow in an excavation-induced fracture network around an underground drift: A case study for a radioactive waste repository in clay rock. *Journal of Hydrology*, **521**, pp.141-156. doi:10.1016/j.jhydrol.2014.11.067

Dewhurst, D.N., Aplin, A.C., and Sarda, J.-P. (1999[1]) Influence of clay fraction on pore-scale properties and hydraulic conductivity of experimentally compacted mudstones. Journal of Geophysical Research, 104, pp. 29,261-29,274.

Dewhurst, D.N., Aplin, A.C., Sarda, J.-P., and Yang, Y. (1998) Compaction-driven evolution of porosity and permeability in natural mudstones: An experimental study. Journal of Geophysical Research, 103, pp. 651-661.

Dewhurst, D.N., Yang, Y., and Aplin, A.C. (1999[2]) Permeability and fluid flow in natural mudstones. In: Aplin, A.C., Fleet, A.J., and Macquaker, J.H.S., eds., Mud and Mudstones: Physical and Fluid Flow Properties, Geological Society of London, Special Publications, 158, pp. 23-43.

Foct, F., Semete, P., Desgree, P., Imbert, C. and Talandier, J. (2012) Hydraulic sealing of fractured argillaceous rocks. *Clays in Natural and Engineered Barriers for Radioactive Waste Confinement*. 5th International Meeting. Montpellier, October 22nd – 25th, 2012.

Gaucher, E.C., Lerouge, C., Blanc, P., and Tournassat, C. (2007) Caractérisation géochimique des forages PAC et nouvelles modélisations THERMOAR. *BRGM*. **RP-54416-FR**.

Gutierrez, M., Øino, L.E. and Nygard, R. (2000) Stress-dependent permeability of a de-mineralised fracture in shale. Marine and Petroleum Geology, 17, pp.895–907.

Harrington, J.F., Cuss, R.C. and Talandier, J. (2017) Gas transport properties through intact and fractured Callovo-Oxfordian mudstones. In: Rutter, E.H., Mecklenburgh, J. & Taylor, K.G. (eds) *Geomechanical and Petrophysical Properties of Mudrocks*. Geological Society, London, Special Publications, **454**. https://doi.org/10.1144/SP454.7

Holt, RM (1990) Permeability reduction induced by a non-hydrostatic stress field. SPE Formation Evaluation, Dec 1990, pp. 444–448.

Katsube, T.J. (2000) Shale permeability and pore-structure evolution characteristics. Geological Survey of Canada. Ottawa, ON, Canada. Pages: 9.

Katsube, T.J., Boitnott, G.N., Lindsay, P.J., and Williamson, M. (1996) Pore structure evolution of compacting muds from the seafloor, offshore Nova Scotia. In: Anonymous, ed., Eastern Canada and national and general programs. Current Research - Geological Survey of Canada, pp. 17-26.

Katsube, T.J., Issler, D.R., and Coyner, K. (1996) Petrophysical characteristics of shale from the Beaufort-Mackenzie Basin, northern Canada; permeability, formation factor, and porosity versus pressure, Interior plains and Arctic Canada. Current Research - Geological Survey of Canada. pp. 45-50.

Katsube, T.J., Mudford, B.S., and Best, M.E. (1991) Petrophysical characteristics of shales from the Scotian shelf. Geophysics, 56, pp.1681-1689.

Keaney, G.M.J., Meredith, P.G., and Murrell, S.A.F. (1998) Laboratory study of permeability evolution in a 'tight' sandstone under non-hydrostatic stress conditions. Rock Mechanics in

Petroleum Engineering, 1 8-10 July 1998, Trondheim, Norway, Society of Petroleum Engineers, SPE/ISRM 47265, pp. 329-335.

Kwon, O., Kronenberg, A.K., Gangi, A.F., and Johnson, B. (2001) Permeability of Wilcox Shale and its effective pressure law. Journal of Geophysical Research, B, Solid Earth and Planets, 106, pp. 19,339-19,353.

Morrow, C., Shi, L.Q., and Byerlee, J.D. (1984) Permeability of fault gouge under confining pressure and shear stress. Journal of Geophysics Research, 89, pp. 3193-3200.

Neuzil, C.E., Bredehoeft, J.D. and Wolff, R.G. (1984) Leakage and fracture permeability in the Cretaceous shales confining the Dakota aquifer in South Dakota. In: Proceedings of First C.V. Theis Conference on Geohydrology in Dublin, Ohio. Jorgensen, D.G. and Signor, D.C. (eds.). National Water Well Association. pp.113-120.

Rutqvist, J., Börgesson, L., Chijimatsu, M., Hernelind, J., Jing, L., Kobayashi, A., and Nguyen, S. (2009) Modeling of damage, permeability changes and pressure responses during excavation of the TSX tunnel in granitic rock at URL, Canada. Environmental Geology, 57 (6), pp. 1263-1274.

Sathar, S., Reeves, H.J., Cuss, R.J., and Harrington, H.J. (2012) Critical stress theory applied to repository concepts; the importance of stress tensor and stress history in fracture flow. Mineralogical Magazine. December 2012, 76 (8), pp. 3165-3177.

Schloemer, S., and Krooss, B.M. (1997) Experimental characterisation of the hydrocarbon sealing efficiency of cap rocks. Marine and Petroleum Geology, 14, pp. 565-580.

Walsh, J.B., and Brace, W.F. (1984) The effect of pressure on porosity and the transport properties of rock. Journal of Geophysical Research. B, 89, pp. 9425-9431.

Yven, B., Sammartino, S., Géraud, Y., Homand, F., and Villiéras, F. (2007) Mineralogy, texture and porosity of Callovo-Oxfordian argillites of the Meuse/Haute-Marne region (eastern Paris Basin). *Mémoires de la Société géologique de France*, **178**, pp.73–90.

Zhang, C.-l., Czaikowski, O., Rothfuchs, T., and Wieczorek, K. (2013) Thermo-Hydro-Mechanical Processes in the Nearfield around a HLW Repository in Argillaceous Formations; Volume I: Laboratory Investigations May 2007 to May 2013. *GRS report*, **GRS-312**, 342pp., ISBN 978-3-939355-91-5

Zhang, C. and Rothfuchs, T. (2004) Experimental study of the hydro-mechanical behaviour of the Callovo-Oxfordian argillite. Applied Clay Science, 26(1), pp.325-336.

Zhu, W., and Wong, T.f. (1994) Permeability evolution related to the brittle-ductile transition in Berea Sandstone. In: Anonymous, ed., AGU 1994 fall meeting., 75; 44 Suppl.: Eos, Transactions, American Geophysical Union. pp. 638.

Zhu, W., and Wong, T.-f. (1997) The transition from brittle faulting to cataclastic flow; permeability evolution. Journal of Geophysical Research, B, Solid Earth and Planets, 102, pp. 3027-3041.

Zoback, M.D., and Byerlee, J.D. (1975) The effect of microcrack dilatancy on the permeability of Westerly Granite. Journal of Geophysics Research, 80, pp. 752-755.

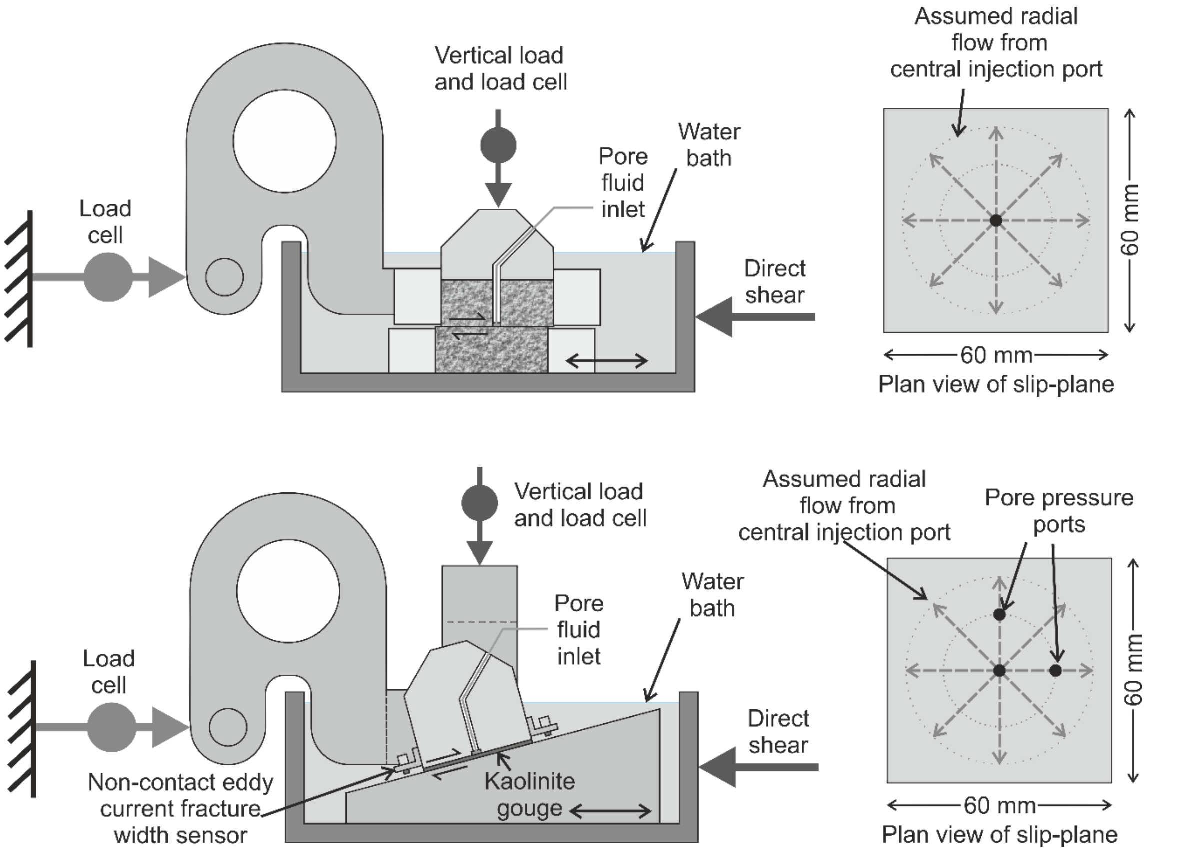

a.
b.

Figure 1 Schematic of the (a) Direct Shear Rig and (b) Angled Shear Rig experimental apparatus.

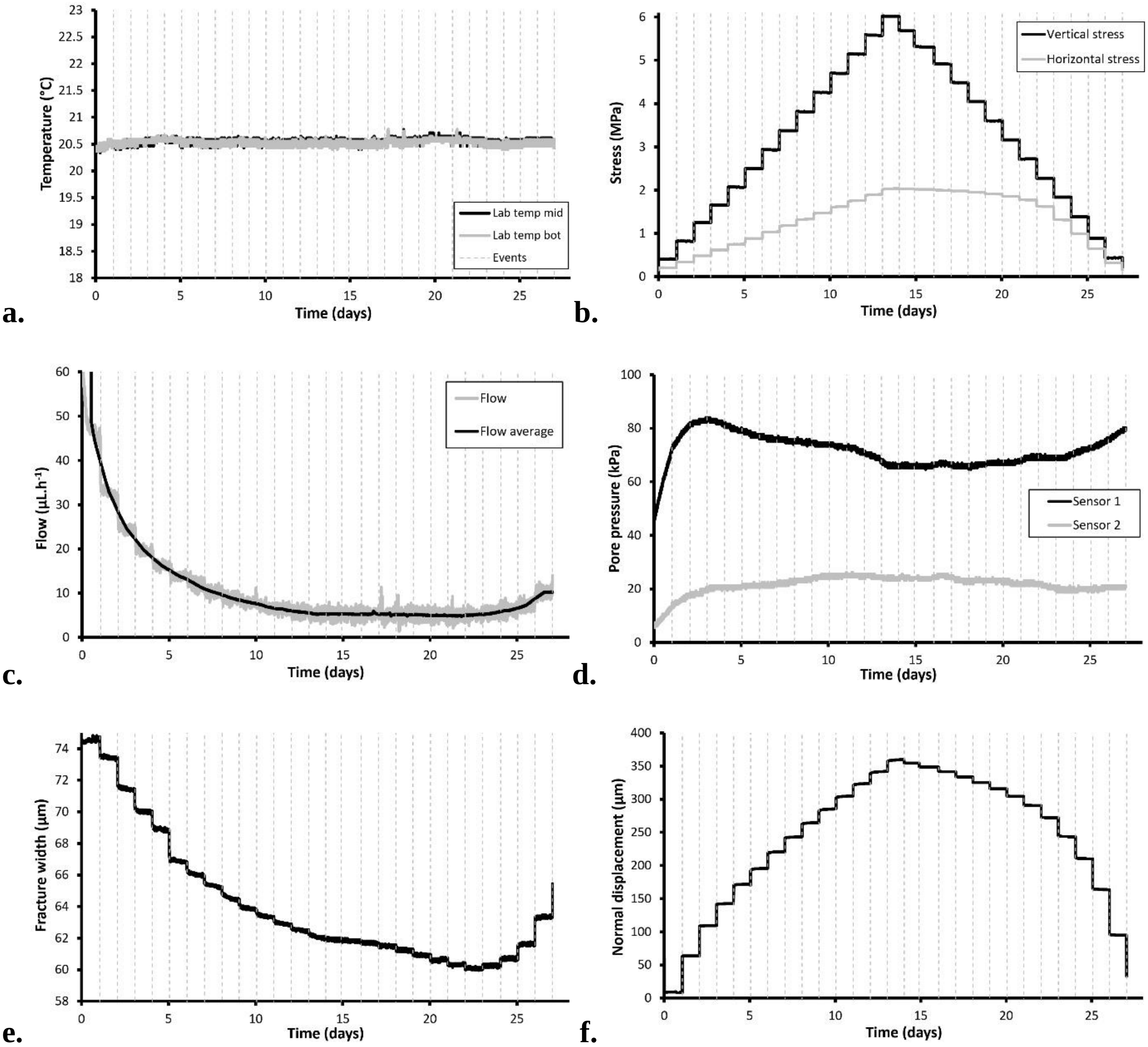

Figure 2 Example results from a hydraulic test conducted on a kaolinite gouge plotted against time (ASR_Tau05_30wLU): a) Temperature; b) Vertical and horizontal stress; c) Hydraulic flow; d) Pore pressures within the slip plane; e) Fracture width; f) Normal displacement.

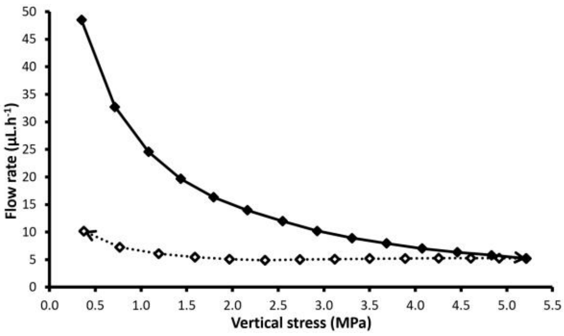

a.

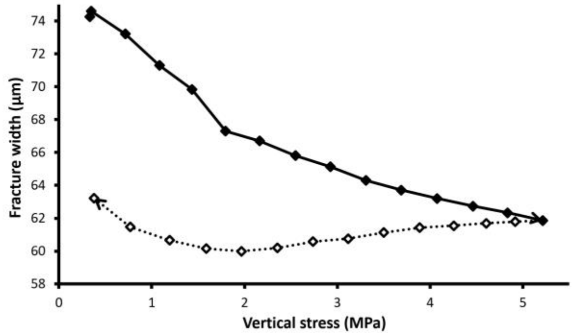

b.

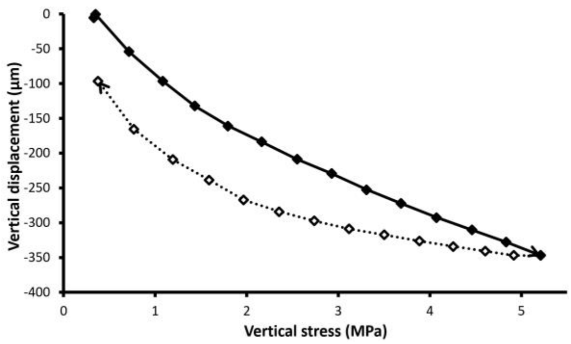

c.

Figure 3 Example results from a hydraulic test conducted on a kaolinite gouge plotted against vertical stress (ASR_Tau05_30wLU): a) Hydraulic flow; b) Fracture width; c) Normal displacement.

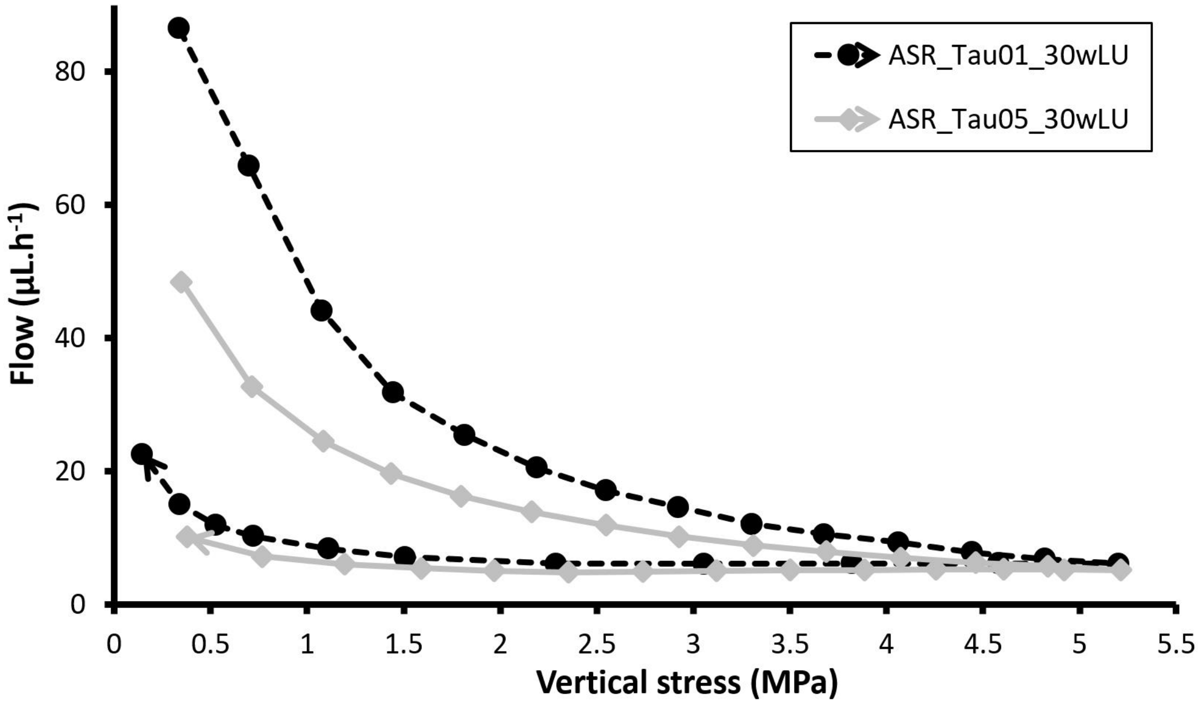

Figure 4 Comparison of two tests conducted on kaolinite gouge showing hysteresis in hydraulic flow during loading/unloading experiments on a 30° slip-plane.

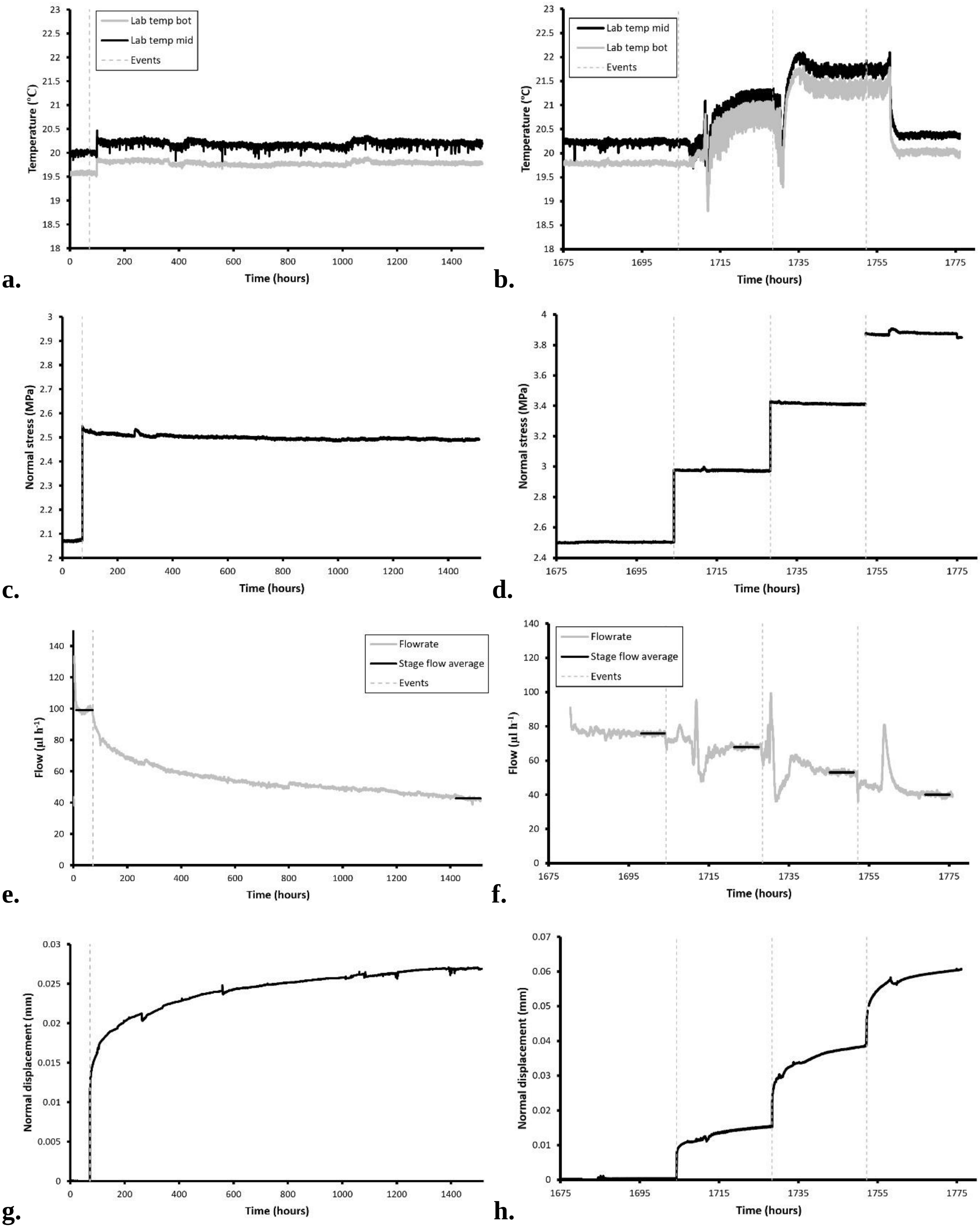

Figure 5 Results from hydraulic test DSR_COx_01 conducted on COx plotted against time: a-b) Temperature; c-d) Normal stress; e-f) Hydraulic flow; g-h) Normal displacement. Figure a, c, e and f represent stage 1 of the test, whilst b, d, f, h represent stage 2.

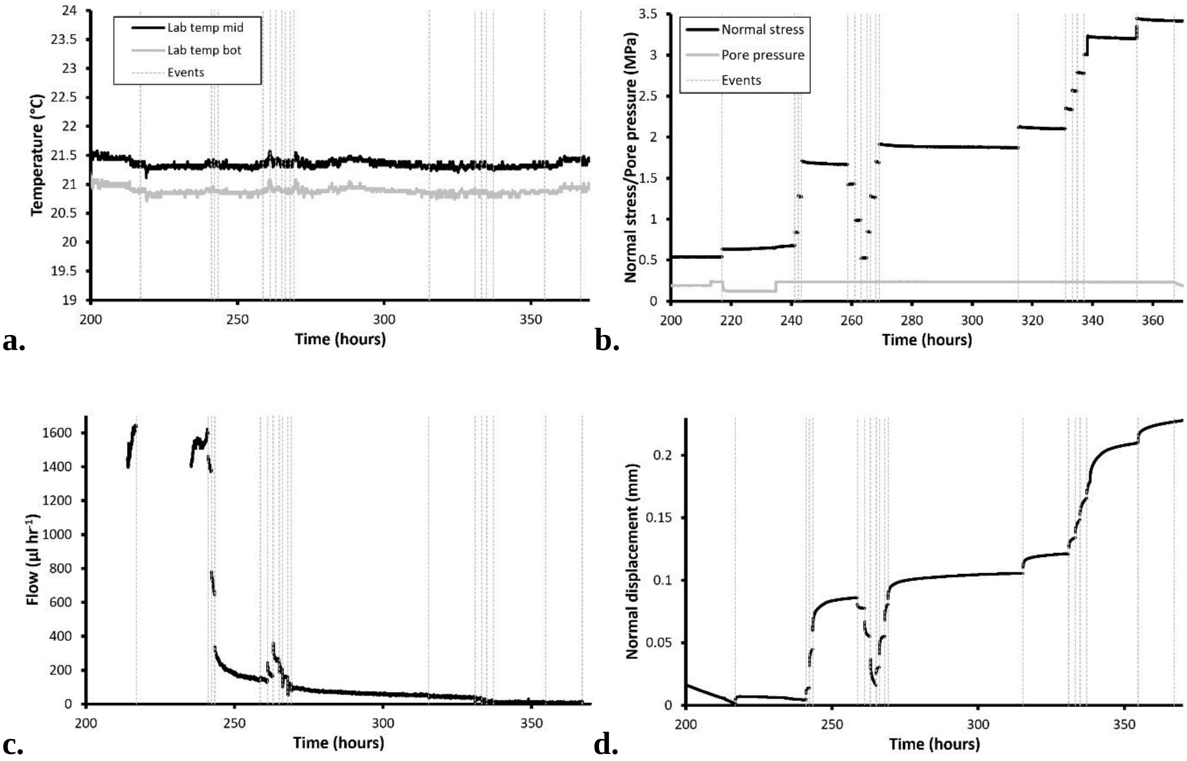

Figure 6 Results from hydraulic test DSR_COx_02 conducted on COx plotted against time: a) Temperature; b) Normal stress and pore pressure; c) Hydraulic flow; d) Normal displacement.

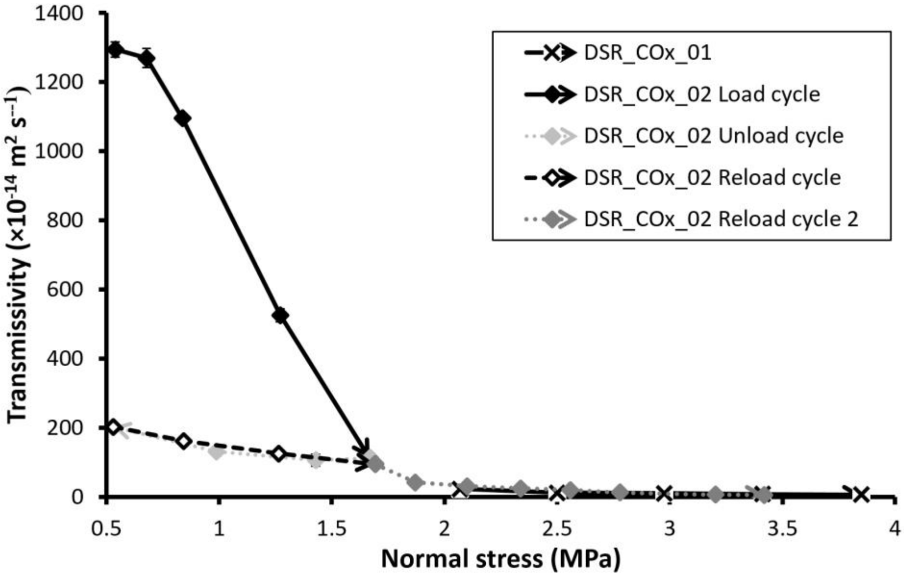

a.

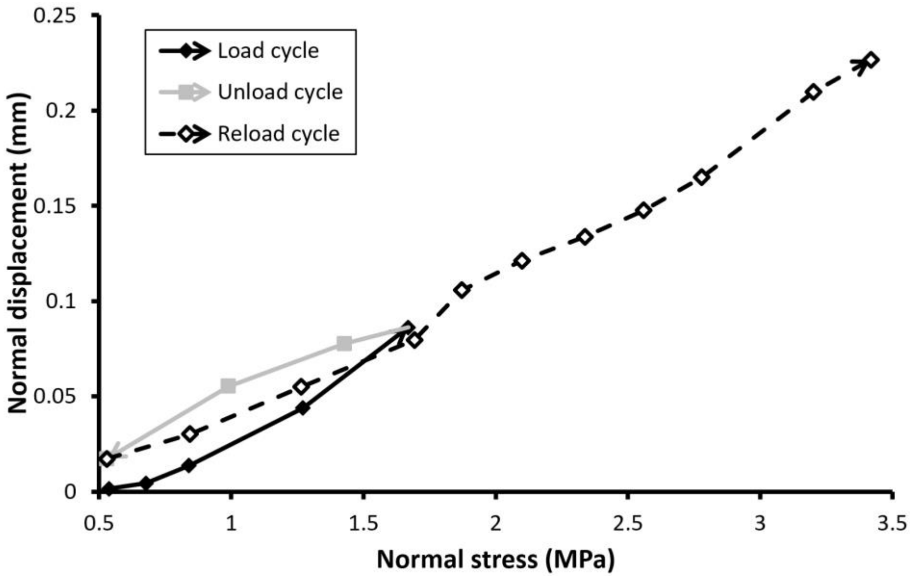

b.

Figure 7 Results from two hydraulic tests conducted on fractured COx against vertical stress: a) Hydraulic flow; b) Normal displacement (Note: test DSR_COx_02 only).

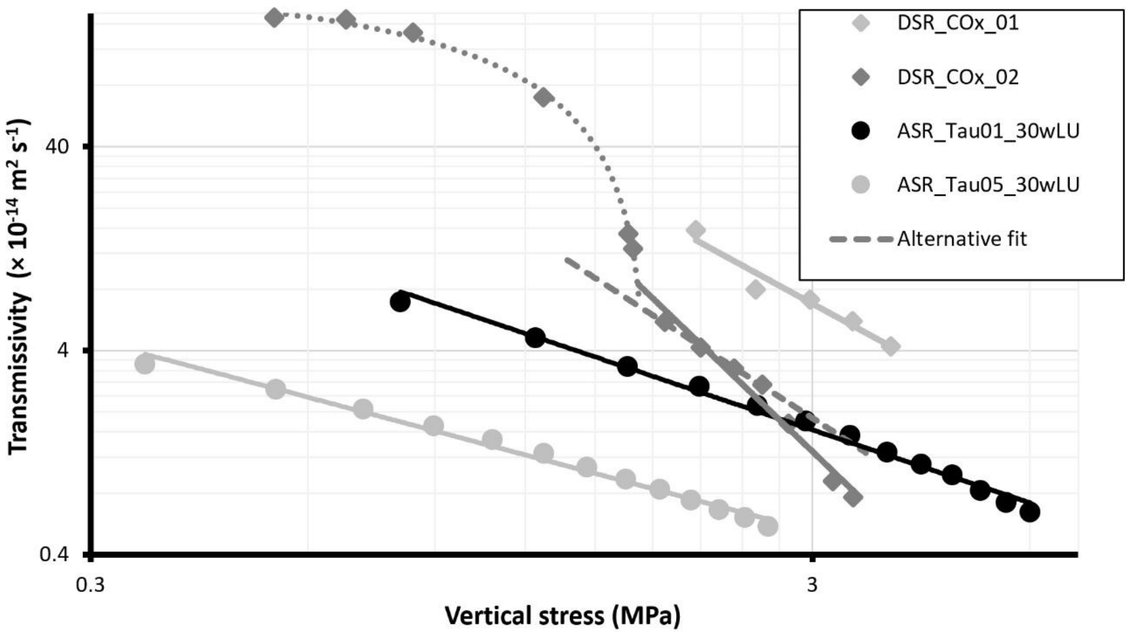

a.

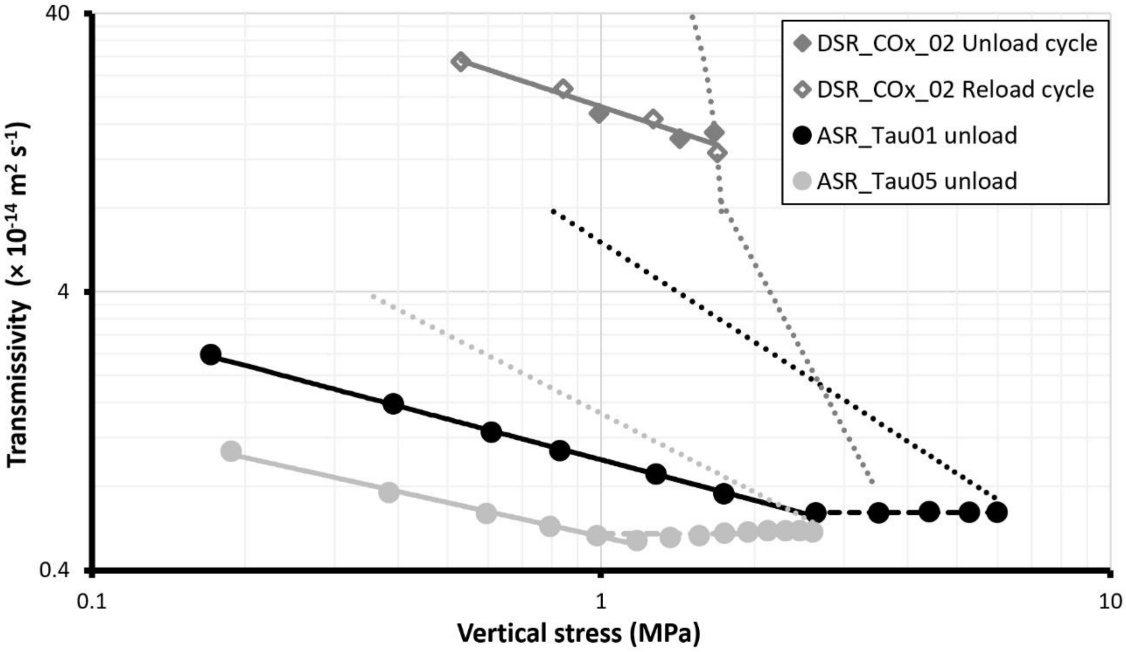

b.

Figure 8 Results for relationship of fracture transmissivity with vertical stress in fractured COx: a) loading response; b) unloading.

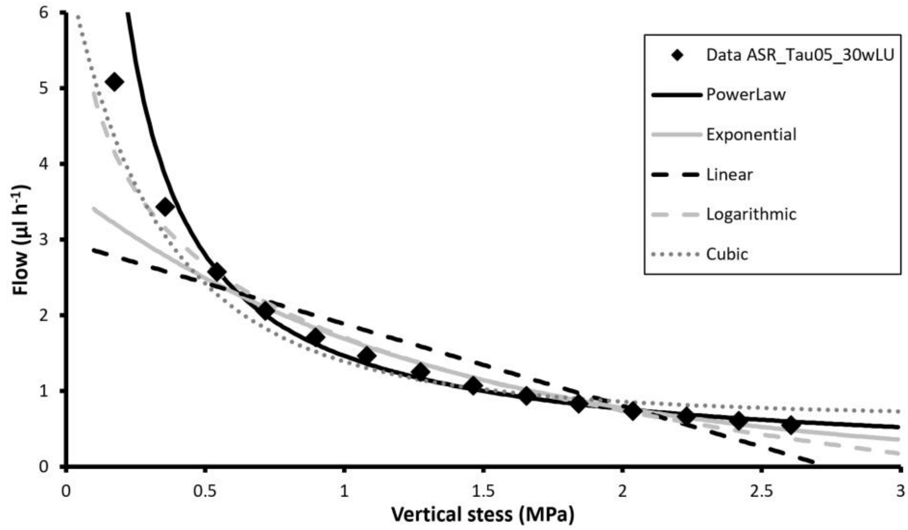

a.

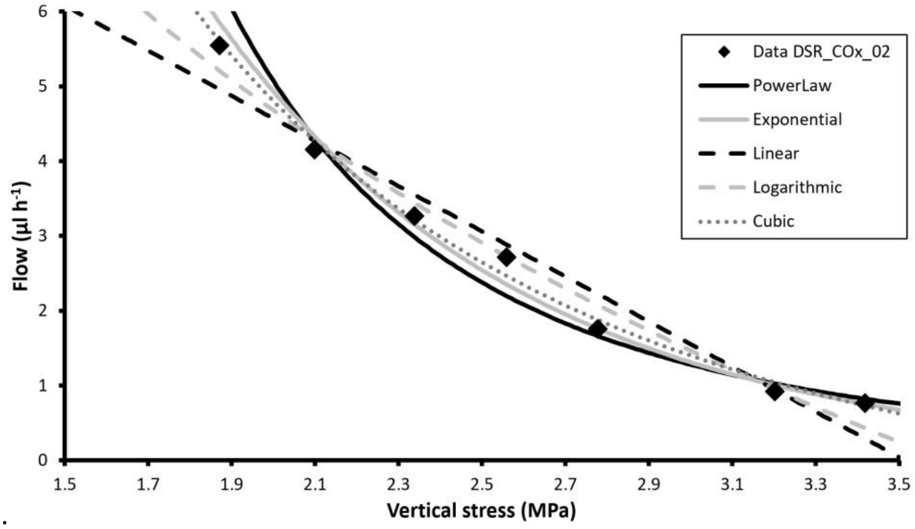

b.

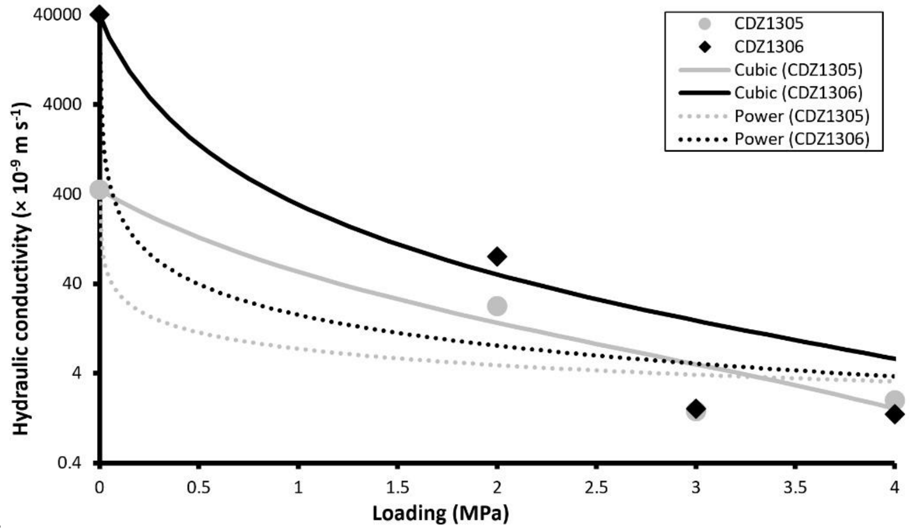

c.

Figure 9 Comparing five best-fit relationships to the experimental data; a) test ASR_Tau05, b) DSR_COx_02. The power-law fit is seen to best describe the data, especially at the initial loading stage at low vertical stress, c) Cubic-law fit to test data from the in situ Compression of the Damage Zone (CDZ) test conducted at the Meuse/Haute-Marne URL (de La Vaissière et al., 2015).

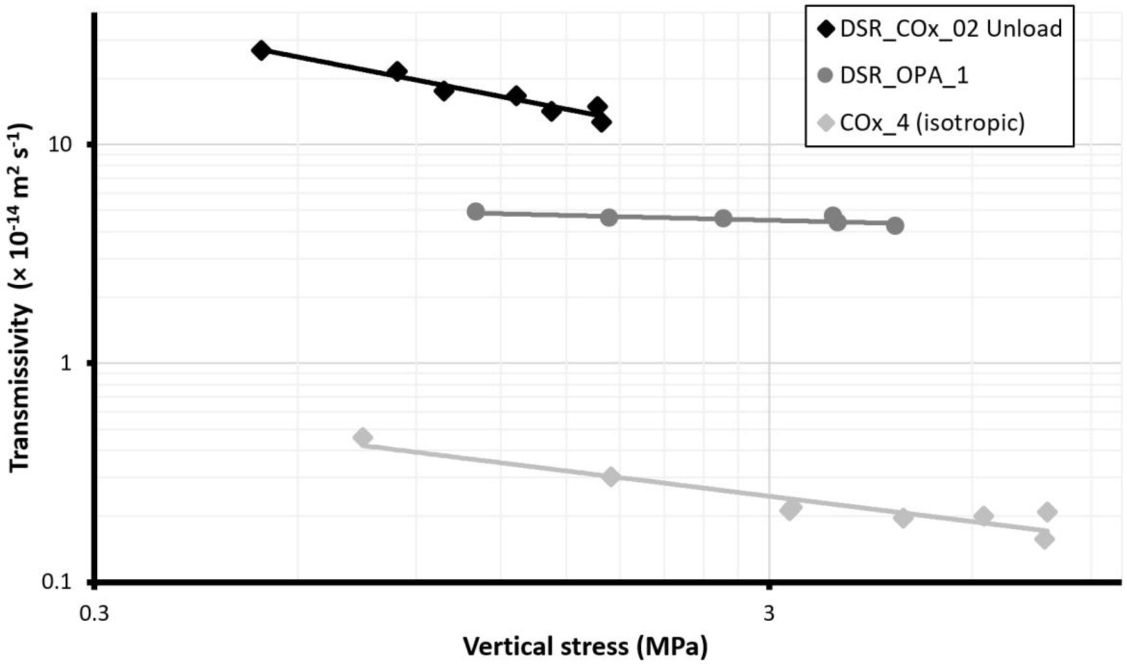

Figure 10 Flow history observed during unload testing of fractures in COx and Opalinus Clay.

	DSR_COx_01	DSR_COx_02
Borehole	OHZ1607	OHZ1607
Sample number	EST44339	EST44342
Borehole depth	8.37 – 8.67 m	9.08 – 9.38 m
Date drilled	21/10/11	21/10/11
Drilling direction	Horizontal	Horizontal
Sample preparation	5/11/13	10/11/14
Sample orientation with respect to bedding	Perpendicular	Parallel
Sample dimensions (mm)	59.9 × 60.1 × 54.3	60.0 × 59.9 × 50.2
Weight (g)	470.6	426.1
Volume (cc)	195.5	181.1
Density (g/cc)	2.43	2.37
Porosity (%)	14.9	17.7
Saturation	0.935	0.80

Table 1 Properties of core and sample material for shear tests conducted on COx.

Experiment	Start date	Sample Material	Water saturation (%)	Fault orientation
ASR_Tau01_30wLU	09-Nov-10	Kaolinite	98	30°
ASR_Tau05_30wLU	27-May-11	Kaolinite	98	30°
DSR_COx_01	6-Nov-13	COx	93.5	0°
DSR_COx_02	10-Nov-14	COx	92.0	0°

Table 2 List of experiments described in the current study. ASR = Angled Shear Rig; DSR = Direct Shear Rig; w = hydraulic test; LU = Load-unload experiment; COx = Callovo-Oxfordian mudstone.

Experiment	Loading	Unloading
ASR_Tau01_30wLU	$6.0\ \sigma_n^{-1.2}$	$1.0\ \sigma_n^{-0.5}$
ASR_Tau05_30wLU	$1.5\ \sigma_n^{-1.0}$	$0.5\ \sigma_n^{-0.4}$
DSR_COx_01	$56\ \sigma_n^{-1.9}$	-
DSR_COx_02	$53\ \sigma_n^{-3.4}$	$18.5\ \sigma_n^{-0.6}$
DSR_COx_02 (alternative)	$23\ \sigma_n^{-2.3}$	-

Table 3 Power-law relationships derived for loading and unloading sections of the experimental data. Note: fit to flow ($\mu l\ h^{-1}$) data.

Experiment		Power-law	Exponential	Logarithmic	Linear	Cubic
ASR_Tau01_30wLU	L	**0.99**	0.97	0.94	0.76	**0.99**
	U	0.94	0.63	0.86	0.50	**0.99**
ASR_Tau05_30wLU	L	**0.99**	0.97	0.98	0.83	**0.99**
	U	0.73	0.41	0.71	0.39	**0.98**
DSR_COx_01	L	0.94	0.92	0.86	0.80	**0.95**
DSR_COx_02	L	0.86	0.94	0.96	**0.99**	
	L	0.97	**0.99**	0.98	0.95	0.91
	U	0.94	0.91	0.95	0.89	**0.99**
Average		0.92	0.84	0.90	0.77	**0.97**
Average load	L	**0.97**	0.96	0.94	0.84	0.96
Average unload	U	0.87	0.65	0.84	0.59	**0.99**

Table 4 Comparison of R^2 values for best-fit relationships for loading (L) and unloading (U) sections of the experimental data.